Dang *et al. Chem Synth* 2023;3:14
DOI: 10.20517/cs.2022.33

Chemical Synthesis

Review

Open Access

Selenium nanomaterials enabled flexible and wearable electronics

Chao Dang[1], Mingyang Liu[1], Zhiwei Lin[1], Wei Yan[1,2,3,*]

[1]School of Electrical and Electronic Engineering, Nanyang Technological University, Singapore 639798, Singapore.
[2]School of Materials Science and Engineering, Nanyang Technological University, Singapore 639798, Singapore.
[3]State Key Laboratory for Modification of Chemical Fibers and Polymer Materials, College of Materials Science and Engineering, Donghua University, Shanghai 201620, China.

***Correspondence to:** Prof./Dr. Wei Yan, School of Electrical and Electronic Engineering, Nanyang Technological University, 50 Nanyang Avenue, Singapore 639798, Singapore. E-mail: wei.yan@ntu.edu.sg

How to cite this article: Dang C, Liu M, Lin Z, Yan W. Selenium nanomaterials enabled flexible and wearable electronics. *Chem Synth* 2023;3:14. https://dx.doi.org/10.20517/cs.2022.33

Received: 23 Oct 2022 **First Decision:** 26 Dec 2022 **Revised:** 2 Feb 2023 **Accepted:** 7 Mar 2023 **Published:** 20 Mar 2023

Academic Editors: Aicheng Chen, Bao-Lian Su **Copy Editor:** Ying Han **Production Editor:** Ying Han

Abstract

Selenium (Se), as an intriguing chalcogenide semiconductor, has traditionally been used for solar energy harvesting. The recent development of nanoscience and nanotechnology has enabled a myriad of Se nanomaterials with compelling structures and unique features. Compared with other chalcogens, Se nanomaterials possess anisotropic crystalline structure, intrinsic chirality, and high reactivity, as well as unique optical, electrical, photoconductive, and piezoelectrical properties. The integration of these Se nanomaterials with technologically important materials, such as conductors and semiconductors, over flexible, bendable, stretchable, and highly curved substrates offer a new generation of Se nanomaterial-based flexible and wearable electronics. In this mini review, we survey the recent scientific and technological breakthroughs in Se nanomaterials-enabled flexible and wearable electronics. We highlight the synthesis, fabrication, morphologies, structure, and properties (optical, electrical, optoelectrical, photovoltaic, and piezoelectric) of Se nanomaterials as well as their integration into innovative functional devices that deliver higher forms of applications across smart sensing, health care, and energy domains. We conclude with a critical analysis of existing challenges and opportunities that will trigger the continued progress of the field.

Keywords: Selenium, Nanomaterials, Flexible electronics, Wearable electronics, Functional fibers

INTRODUCTION

Flexible and wearable electronics capable of continuous monitoring of physiological signals[1-5], minimally invasive interrogation of neural circuitry[6-10], and performing diagnostic and therapeutic treatment[11-15] are offering unprecedented value to society and our everyday lives[16-20]. Functional materials that are responsive to stimuli (such as photons[21-25], stress[26-30], and chemicals[31-34]) are the core part of flexible and wearable electronics[35-37]. The incorporation of semiconducting materials with excellent electrical and optical properties into flexible and wearable electronics enables innovative smart devices and systems with powerful potential in personalized healthcare, precision medical surgery and large-area energy harvesting and storage[38-40]. Selenium (Se) is a trace element of group VI with a direct bandgap at room temperature[41]. Due to its unique band structure and crystal structure, Se, in its bulky form, shows attractive optical, electrical, electronic and piezoelectric properties opening up interesting applications in photodetection and solar energy harvesting[42-44]. Compared with typical semiconductors in electronic industry (such as silicon and germanium) that require sophisticated micro- and nanofabrication conditions, Se can be physically, thermally or chemically processed in simple, low-cost and robust manners, which makes its integration with flexible and wearable electronics straightforward, thereby enabling versatile devices and applications[45,46].

Thanks to the remarkable progress in nanofabrication and nanotechnology, bulky Se can be scaled down to tunable nanostructures ranging from zero-dimensional (0D) nanoparticles to two-dimensional (2D) nanosheets. Benefiting from the "nano-size" effect, Se nanomaterials exhibit distinct physical and chemical properties that cannot be found in their bulky counterparts, featuring improved mechanical, electrical, thermal, optical and piezoelectric performance[47-49]. Compared with other functional semiconducting nanomaterials such as Si nanowires, Ge nanowires and ZnSe nanowires employed in flexible electronics[50], Se nanomaterials show the distinctive advantage of processability. They can be easily integrated with traditional conductors and semiconductors over the flexible, bendable, stretchable, and highly curved substrates to fabricate innovative functional devices in the form factors of two-dimensional large-area films and patches as well as one-dimensional indefinitely long fibers as we elaborated in the section of "APPLICATIONS OF SELENIUM NANOMATERIALS IN FLEXIBLE AND WEARABLE ELECTRONICS". This allows for the development of a new generation of Se nanomaterial-based flexible and wearable electronics. This mini review highlights the recent advances in Se nanomaterials enabled flexible and wearable electronics. We will first briefly review the typical morphologies and crystal structure of Se nanomaterials that directly determine their properties and subsequent applications. We will then present the synthesis and fabrication methodologies of Se nanostructures, namely the "bottom-up" and "top-down" strategies that have been widely exploited in the nanofabrication field. In the next section, we will discuss the physical properties of Se nanomaterials, focusing on optical, electrical, optoelectrical, photovoltaic, and piezoelectric behaviors that are of great importance for their functional applications in flexible and wearable electronics. Finally, we will discuss how Se nanomaterials can be integrated with substrates that are flexible, bendable, large-area and highly curved and how these innovative devices open up interesting opportunities in photosensing, mechanical deformation sensing, physiological sensing and energy storage. The review concludes with some key remaining challenges and perspectives that will be of value for future advances and breakthroughs in the field.

MORPHOLOGIES AND CRYSTAL STRUCTURES OF SELENIUM NANOMATERIALS

The morphologies, sizes and crystal structure of materials determine their properties and applications. We begin with a brief introduction to the morphologies and structure of Se nanomaterials.

Generally, nanostructured Se can be categorized into zero-dimensional (0D), one-dimensional (1D), and two-dimensional (2D) form factors, as shown by the microscopic images in Figure 1 and Table 1. 0D Se

Table 1. Summary of some representative synthesis methods, structures, properties, and applications of the Se nanomaterials

Se morphology	Crystal structures	Synthesis methods	Precursors	Reaction conditions	Properties	Applications	Refs.
0D nanoparticles	Hexagonal structure	Chemical reduction	Sodium selenite	Water, 2 ± 8 °C, 72 h	Anti hydroxyl radical property	Anti-oxidative stress drugs	[52]
0D nanoparticles	Hexagonal structure	Solvent-thermal method	Selenous acid	Ethanol and distilled water, 150 °C, 24 h	Fluorescence property	Fluorescence sensors	[64]
0D nanoparticles	Hexagonal structure	Laser-ablation method	Solide Se	Water, radiation wavelength of 1060 to 1070 nm, pulse repetition rate of 20 kHz, pulse duration of 80 ns	NA	Biological therapy	[65]
0D nanoparticles	Hexagonal structure	Ball Milling and heating	Se bulk	Ball milling, 72 h, heating, 260 °C, 20 h, argon gas atmosphere	Electrical/Electrochemical properties	Li-Se batteries	[104]
1D nanowires	Trigonal structure	Thermally-drawn assisted method	Se core	260 °C, air atmosphere	Optoelectrical property	Fluorescence imaging fibers	[39]
1D nanowires	Trigonal structure	Chemical reduction	SeO_2	Water, room temperature	Electrical property	Li-Se batteries	[53]
1D nanorods	Hexagonal structure	Microwave-polyol method	SeO_2	195 °C, 30 min, microwave heating	NA	NA	[54]
1D nanotubes	Trigonal structure	Hydrothermal method	Sodium selenite	Water, 100 °C, 25 h	NA	NA	[55]
1D nanobelts	Trigonal structure	Chemical reduction	Sodium selenite	Acid condition, 50 °C, 3 h	Optical property	Optical detector	[56]
1D nanowires	Trigonal structure	Self-seeding solution-phase method	Selenious acid	Ice water	Optical/Photoconductivity property	Electronic, optical or mechanical nanodevices	[68]
1D nanowires	Trigonal structure	Plasma-assisted selenization method	Se tank	300 °C, plasma, heating	Optoelectrical property	Flexible photodetectors	[69]
1D nanowire /nanotube	Trigonal structure	Thermally-drawn assisted method	Se rod	260 °C, 30 min	Photoconductivity property	Optoelectronic detectors	[70]
1D nanowires	Trigonal structure	Solvent-thermal method	SeO_2	Water and ethanol, 160 °C, 20 h	Piezoelectric property	Piezoelectric nanogenerators	[85]
1D nanobelts	Trigonal structure	Thermal evaporation method	Se powder	250 °C, 1 h, argon gas atmosphere	Electrical/ Photoconductivity property	Visible light photodetector	[94]
2D nanosheets	Trigonal structure	Physical vapor deposition method	Se powder	210 °C, 60 min argon atmosphere	Photoelectrical property	Phototransistors	[57]
2D nanolayers	Hexagonal structure	Chemical vapor transport synthesis	Se powder	Liquid phase, hydrogen and argon gas atmosphere	NA	NA	[71]
2D nanoflakes	Trigonal structure	Sonication liquid-phase exfoliation method	Bulk Se powder	IPA, 9 h, energy power of 600 W	Fluorescence property	Photoluminescence	[58]

nanomaterials include Se nanospheres and Se nanoparticles[51,52]. The synthesis method, surfactant or additive, reaction temperature, or reaction time influences their morphologies and properties. 1D Se nanomaterials have attracted lots of research interest recently because of their unique optical and electrical properties as well as potential employment in flexible electronics. A number of well-established techniques, mostly derived from "top-down" and "bottom-up" strategies, have been adopted to produce 1D nanostructures, including nanowires, nanorods, nanotubes, and nanobelts[53-56]. Compared with 1D metal nanomaterials, 1D Se nanomaterials show competitive advantages in terms of synthesis methodologies,

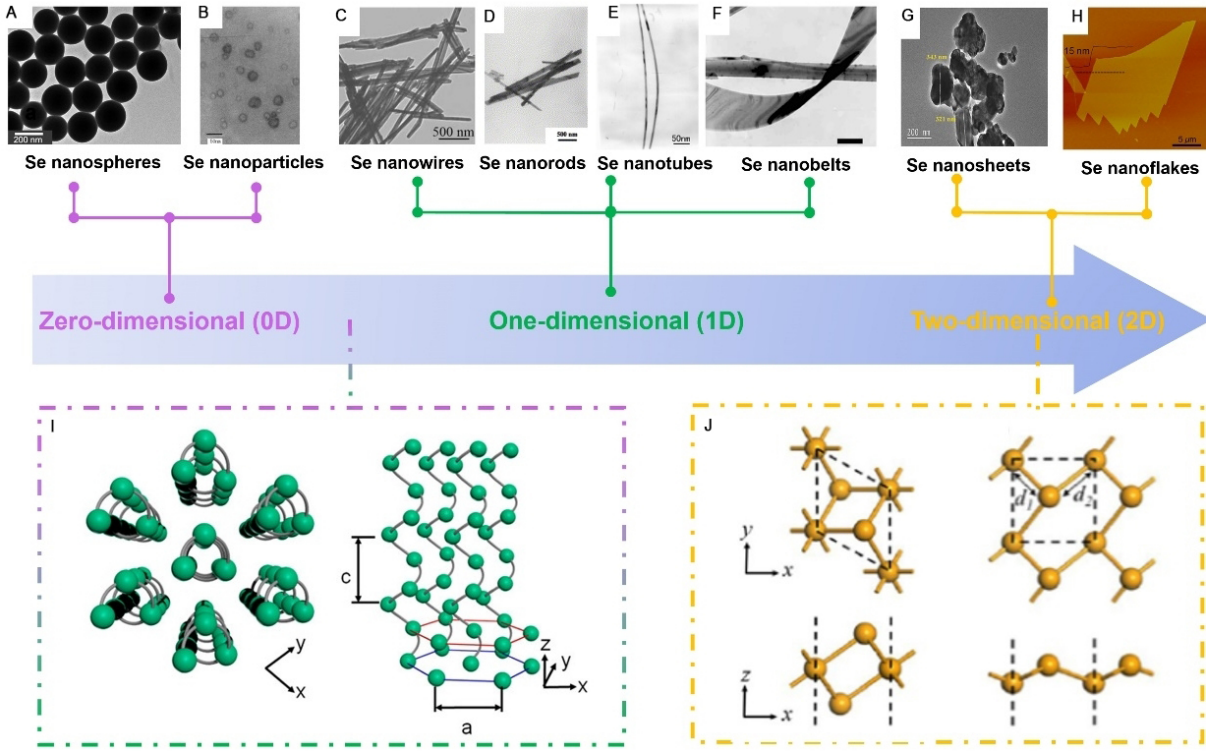

Figure 1. (A) TEM image of Se nanosphere[51]; Copyright 2014, Elsevier. (B) TEM image of Se nanoparticles[52]; Copyright 2002, Wiley-VCH. (C) TEM image of Se nanowires[53]; Copyright 2015, Elsevier. (D) TEM image of Se nanorods[54]; Copyright 2004, Elsevier. (E) SEM image of Se nanotube[55]; Copyright 2006, American Chemical Society. (F) TEM image of Se nanobelts[56]; Copyright 2005, American Chemical Society. (G) TEM image of Se nanosheets[57]; Copyright 2017, American Chemical Society. (H) AFM topography image of Se nanoflakes[58]; Copyright 2017, Wiley-VCH. (I) Hexagonal structure existed in 0D and 1D Se nanomaterials[57]; Copyright 2002, Wiley-VCH. (J) 1T-MoS_2-like structure and square structure existed in 2D Se nanomaterials[60]; Copyright 2022, Springer.

structural and morphological tunability, and volumetric dispersion. Considerable efforts have been made to develop 2D Se nanomaterials since the emergence of Se nanoflakes in 2017[57]. 2D nanostructures have been demonstrated to be crucial and more suitable for device applications thanks to their high specific surface area, carrier capacity, energy storage ability, conversion efficiency, and environmental stability[58,59]. 2D Se nanomaterials offer a huge number of active sites on the surface for storing and transporting ions, thus acting as active electrode materials in energy storage systems[59].

Se has six allotropic forms that can be classified as either crystalline or amorphous in the solid state based on its molecular structure[60,61]. There are five types of crystalline phases, including hexagonal Se with thermodynamic stability, a, b, c-monoclinic Se, rhombohedral Se, orthorhombic Se, and a and b-cubic Se. Non-crystalline allotropes of Se can be classified as amorphous and vitreous forms. The red and black amorphous Se is formed based on Se_8 rings and Se_8 chains, respectively, while vitreous Se is established on Se_8 chains[62]. The chain arrangement greatly affects the electronic structure of Se[63]. For instance, monoclinic, amorphous, or another metastable Se is insulating. In contrast, trigonal Se is semiconducting. The atoms in trigonal Se are covalently bonded into spiral chains oriented along the c-axis, while the adjacent chains are weakly connected via van der Waals interactions and run along their radical directions, leading to a hexagonal structure [Figure 1I], which can facilitate electronic conduction[57]. The hexagonal structure exists in a wide range of 0D and 1D Se nanomaterials, enabling them to be promising semiconductors for optoelectronics and piezoelectronics. Because of the intrinsic anisotropy of the atomic structure, Se is prone to form 0D and 1D nanostructures, while 2D Se nanomaterials are relatively difficult

to fabricate. It is reported that 2D Se nanomaterials have relatively complex structures based on crystal search computations. Besides the hexagonal and trigonal structure, two other stable structures including 1T-MoS_2-like structure (*T*-Se) and square structure (*S*-Se) may exist [Figure 1J][63].

SYNTHESIS STRATEGIES AND FABRICATION TECHNIQUES OF SELENIUM NANOMATERIALS

The synthesis strategies and fabrication techniques greatly dictate the morphologies and structures of the resulting Se. So far, numerous protocols for synthesizing Se nanomaterials, such as chemical reduction, chemical vapor transfer synthesis, and thermally drawn-assisted synthesis, have been reported [Table 1]. The following section analyzes some representative synthesis and fabrication strategies of Se nanomaterials, including nanospheres, nanoparticles, nanotubes, nanowires, and nanosheets.

0D Se nanomaterial

Due to the low cost, biocompatibility, and outstanding electrical properties, 0D Se nanomaterials have been brought into focus in chemical and material communities. Chemical reduction is one of the most common strategies for the synthesis of 0D Se. This approach involves reducing Se salts with various reducing chemicals. Se nanoparticles with a hollow structure synthesized by using A (Pr), sodium selenite, and mercaptothion as a template, Se sources, and reducing agents have been reported [Figure 2A][52]. TEM characterization revealed the hollow structures at the edges and centers. However, the obtained Se nanoparticles contain impurities, transferring these nanoscale materials is complicated, and breaking the serious aggregation remains challenging. All these issues restrict the practical application of these nanoparticles. The emergence of solvothermal synthesis successfully solves the problems, resulting in nanoparticles of high purity, uniform morphologies, and slight aggregation [Figure 2B][64]. Additionally, this method is facile to enable super-small nanoparticles. One example shown in Figure 2B (ii) shows nanoparticles with radii of 3-8 nm. In addition, laser ablation of solid bulky Se at the solid-liquid interface could also be harnessed to produce Se nanoparticles [Figure 2C][65]. With this "top-down" strategy, colloidal Se nanoparticles with sizes of below 100 nm are fabricated in pure water. Such Se nanoparticles are expected to be useful for biological applications. However, some issues that impede the practical application of 0D Se are also reported in these studies. For example, the collision and aggregation of Se nanoparticles frequently occurred, which easily led to serious surface oxidation and degradation. The research on oxidation and degradation will be at the center of the solvothermal synthesis of 0D Se nanomaterials.

1D Se nanomaterials

1D Se nanomaterials such as nanowires, nanorods, nanotubes, and nanobelts have elicited significant interest because of their outstanding optical and electrical properties. Two strategies, namely the "top-down" and "bottom-up" approaches, have been generally employed for the synthesis of 1D formats. Specifically, the "top-down" strategy relies on selective removal of material from a solid bulky Se in a subtractive manner, while the "bottom-up" strategy utilizes individual atoms as the building blocks to realize structure assembling in an additive fashion[66,67].

1D Se nanomaterials are commonly fabricated with the "bottom-up" approach because the atomic composition, size, and shape can be tailorable and controllable. This approach typically involves the decomposition of Se-based compound via chemical reactions either at room or an elevated temperature [Figure 3A]. The resulting nanowires are highly uniform, large-area and of high aspect ratio [Figure 3A (i)][68]. Their lateral dimensions are controllable depending on the process parameters [Figure 3A (ii)]. However, Se nanowires prepared by this approach can be easily contaminated by the used chemical reagents. In addition, the relatively poor crystallinity and high density of defects further frustrate

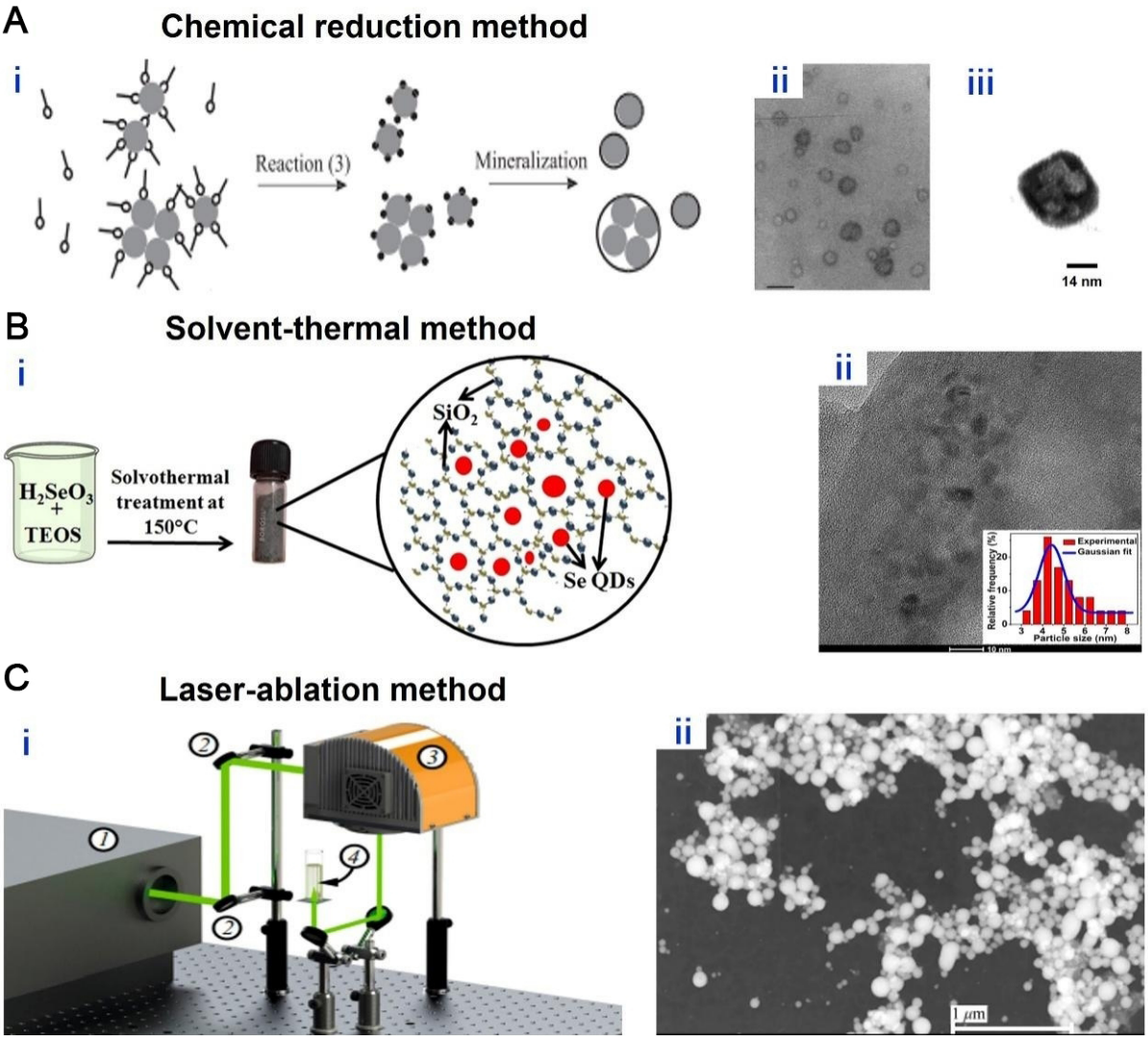

Figure 2. (A) (i) Schematic illustration of the chemical reduction method[52]; (ii) TEM image of hollow sphere Se nanoparticles; (iii) HRTEM image of a hollow sphere Se nanoparticle; Copyright 2002, Wiley-VCH. (B) Scheme illustration of the solvent-thermal method[64]; (i) Large-area HRTEM image and the particle size distribution of Se nanoparticles; (ii) HRTEM image of Se nanoparticles showing *d* spacings; Copyright 2021, American Chemical Society. (C) (i) Schematic of the laser-ablation method[65]; (ii) TEM image of selenium nanoparticles; Copyright 2019, Springer.

the device application. In contrast, chemical vapor deposition (CVD), which involves chemical reaction, vapor evaporation, and decomposition, enables the production of defect-free, trigonal Se nanowires. For example, Chen *et al.* developed a reliable strategy for Se nanowires synthesis in a selenization furnace with the aid of plasma [Figure 3B][69]. Upon reaching its vaporization point at 300 °C, the Se tank emitted Se vapor, which flowed towards the plasma coil, creating ionized Se, which is then grown into Se nanowires on an oxidized silicon substrate [Figure 3B (i)]. As displayed by the SEM and TEM images, a forest of Se nanowires was synthesized, and high-quality crystallinity was achieved [Figure 3B (ii)].

Although the bottom-up approach allows the massive production of Se nanowires at a low cost and in an efficient manner, the manipulation of the entangled nanowire mesh and their integration into devices remains challenging. Very recently, an impressive "top-down" route that exploits the thermal drawing

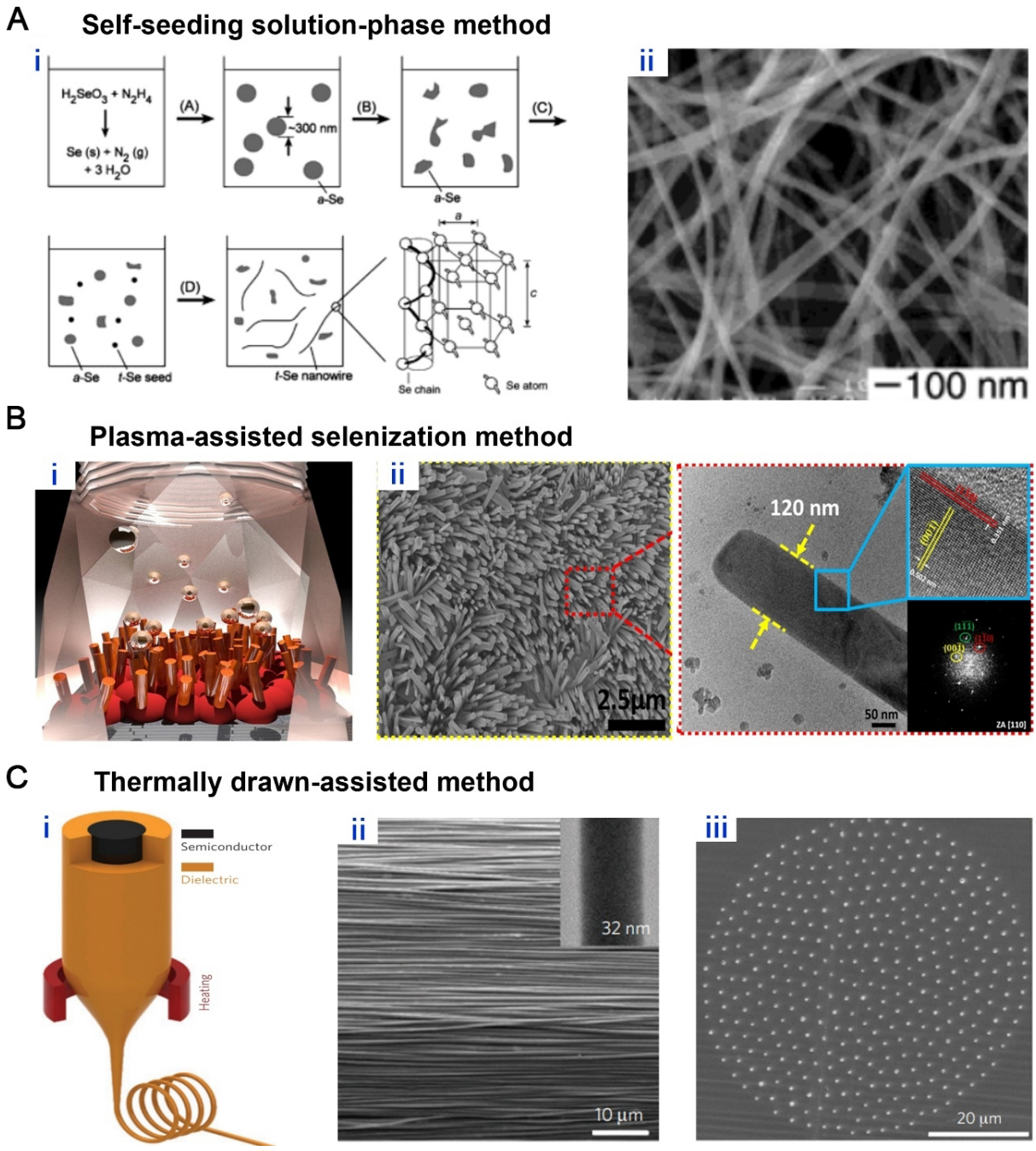

Figure 3. (A) (i) Schematic illustration of self-seeding solution-phase method[68]; (ii) SEM image of Se nanowires; Copyright 2002, Wiley-VCH. (B) (i) Schematic of the plasma-assisted selenization process[69]; (ii) A top view SEM image of Se nanowires and a magnified TEM image of single Se nanowire with the lattice spacings of 0.351 nm of (110) and 0.502 nm of (001); Copyright 2018, American Chemical Society. (C) (i) Schematic illustration of thermally drawn-assisted method[70]; (ii) SEM image of Se nanowire arrays and inset is TEM image of a single nanowire with 32 nm thickness; (iii) Cross-sectional SEM micrograph of Se nanowires; Copyright 2011, Nature Publishing Group.

approach has been developed to fabricate well-ordered, highly uniform Se nanowires and nanotubes [Figure 3C (i)][70]. This method involves multistep iterative co-drawing of Se embedded in a polymeric cladding that supports most of the stress resulting from thermal drawing. Starting with a Se macroscopic

rod that was sealed in a thermoplastic matrix, the first draw scaled down the lateral feature size of Se to a few millimeters. Assembling a bundle of first-drawn fibers and embedding them into a second polymer matrix that was re-drawn reduced the feature size to a few micrometers. A third step finally enabled nanowires and nanotubes with diameters of a few tens of nanometers [Figure 3C (ii)-(iii)]. The nanostructures are radially and axially uniform, axially parallel and indefinitely long, unachieved with any other approaches. Most strikingly, it is very easy to handle these nanostructures and interface them with external electrodes forming flexible electronic devices.

2D Se nanomaterials

2D nanomaterials have attracted exponentially increased academic attention since graphene was discovered. The unique physicochemical properties of 2D nanomaterials make them suitable for use in optoelectronics, electronics, energy storage, and catalysts. Due to Se's intrinsic anisotropic atomic structure, the fabrication of 2D Se nanomaterials remains challenging as opposed to the 0D and 1D Se nanomaterials.

Physical vapor deposition (PVD), a thin-film coating process in which solid materials are vaporized under vacuum conditions and then deposited onto a substrate, has been considered as a promising technique for 2D Se nanomaterials fabrication. Se nanoflakes featured with thicknesses of 5 nm have been fabricated on a Si wafer substrate via depositing Se vapor generated from bulky Se powders [Figure 4A (i)][57]. The nanoflakes were irregularly shaped and zigzagged [Figure 4A (ii)]. Structural characterization reveals the helical atomic chains as well as lattice fringe spacing of typical trigonal structure [Figure 4A (iii)]. Chemical vapor transport (CVT) has also been emerging as one of the promising techniques for 2D Se nanomaterials fabrication[71]. CVT utilizes reversible chemical reactions to trigger crystal growth in different directions at different temperatures. The source materials are easy to obtain, and chemical reactions can be controlled. More importantly, the reactant composition can be easily tailored, thus enabling control over the characteristics of the targeted 2D Se nanomaterials. With this technique, Se nanosheets with typical trigonal crystals have been fabricated [Figure 4B (i)]. The thickness of the monolayer is 0.75 nm [Figure 4B (ii)-(iii)][71].

However, stringent conditions such as ultrahigh vacuum and high temperature frustrate the large-scale production and potential applications of those 2D Se nanomaterials. Exploring more facile and green strategies and techniques is the mainstream direction for future development. Due to their strong in-plane chemical covalent bonds and weak out-of-plane van der Waals interactions, 2D Se nanomaterials can be readily fabricated by the well-established "top-down" methods, such as exfoliating from Se bulk materials in liquid phase. However, it is important to note that the processing temperature should be maintained at 0-10 ℃ in an ice bath, which can prevent the serious oxidation of Se nanostructures. Se nanosheets with ultrathin nanolayered structure have thus been fabricated in an isopropanol solution with probe sonication and centrifugation [Figure 4C (i)][58]. Under a low centrifugation speed, Se nanosheets showed average thicknesses of between 10 and 27 nm, whereas ultrathin features with average thicknesses of 3-6 nm were observed at high centrifugation speeds. TEM characterization revealed the lattice fringe spacings of 0.38, 0.22, and 0.29 nm, which correspond to the crystal plane spacings of (100), (110), and (101) planes [Figure 4C (ii)-(iii)].

PROPERTIES OF SELENIUM NANOMATERIALS

As shown in Table 1, several unique properties of Se nanomaterials, including optical, optoelectronic and piezoelectric properties, and the morphologies and structure-properties relationship are briefly discussed in this section.

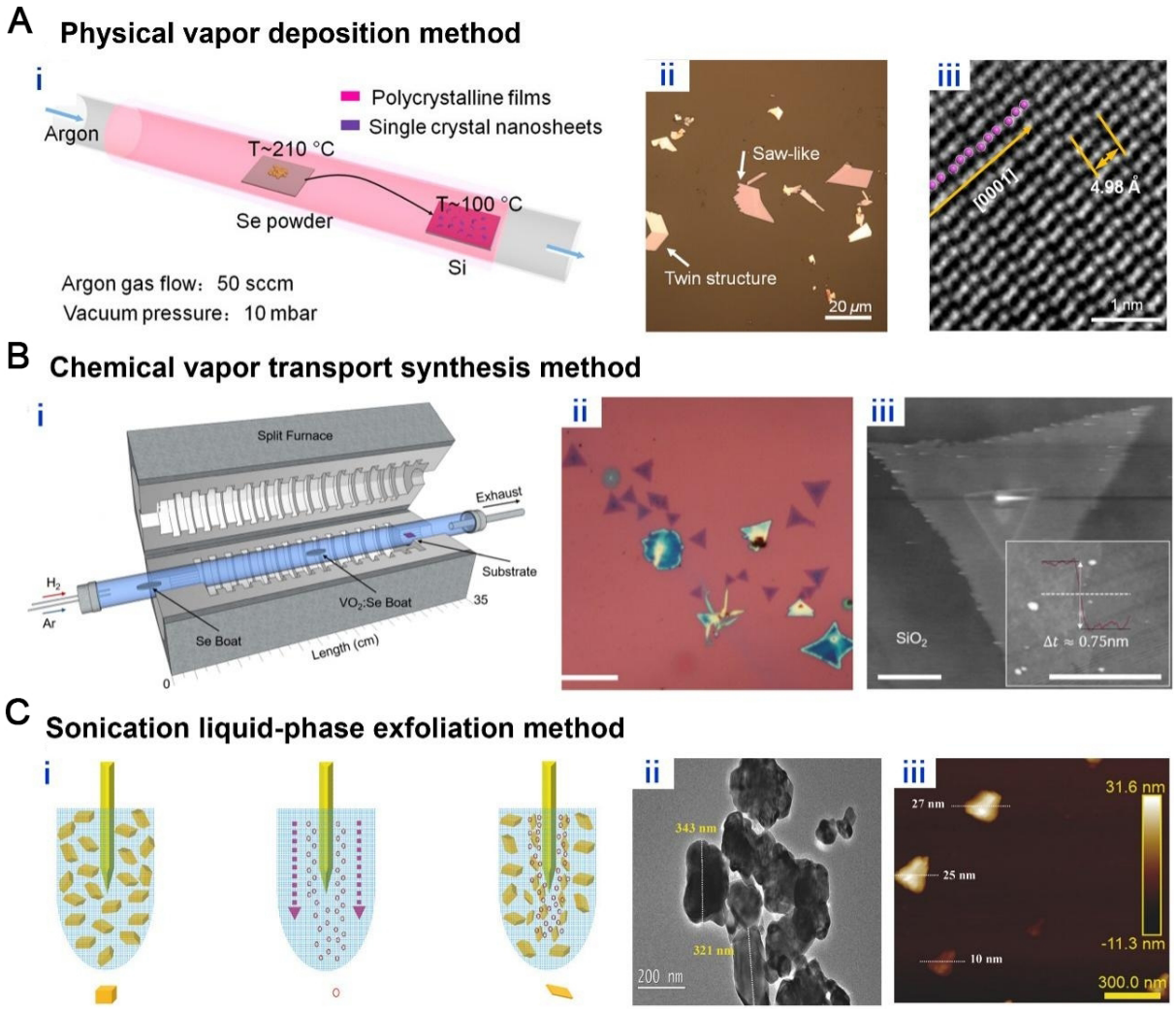

Figure 4. (A) (i) Schematic diagram of the PVD method[57]; (ii) AFM height profile of a twin structure nanosheet; (iii) HAADF-STEM image of Se nanosheets; Copyright 2017, American Chemical Society. (B) (i) Schematic of the CVT method[71]; (ii) Optical microscope image of Se nanoflakes; (iii) AFM image of a Se nanoflake; Copyright 2018, © TÜRKİYE. (C) (i) Schematic demonstration of sonication liquid-phase exfoliation method[58]; (ii) TEM images of Se nanosheets; (iii) AFM images of Se nanosheets; Copyright 2017, Wiley-VCH.

One of the attractive features is tunable and controllable optical properties caused by the quantum confinement effect. The optical properties of Se are of great importance for its photoconductive, photovoltaic and rectifying behaviors and, thus, its device application. Filippo *et al.* found that the UV-vis absorption spectrum of Se microtubes with nanoscale walls consisted of many bands that were typically observed in Se nanowires and some other distinct bands that could be attributed to the interchain interactions perpendicular to the c-axis [Figure 5A][72]. The optical properties of the nanostructured tubes are very different from those of the bulky Se powder source. Moreover, Xing *et al.* found that the optical properties of Se nanoflakes could be modulated through sonication treatments that affected the concentration of the formed Se nanoflakes, as demonstrated by the tunable optical absorbance versus sonication time [Figure 5B (i)][58]. Because of the fluorescence quenching effect and the equilibration of lateral sizes of Se nanoflakes, a new fluorescence emission peak appeared at 367 nm after 3.5 h sonication [Figure 5B (ii)]. The bandgap of Se nanoflakes ranged from 1.8 to 2.2 eV, making it a promising transition semiconductor. Based on electronic structure calculations, it is found that Se nanoflakes with 1T-MoS_2-like structure and tiled helical-chain structure had an indirect bandgap of 1.11 eV and 2.64 eV, respectively[60].

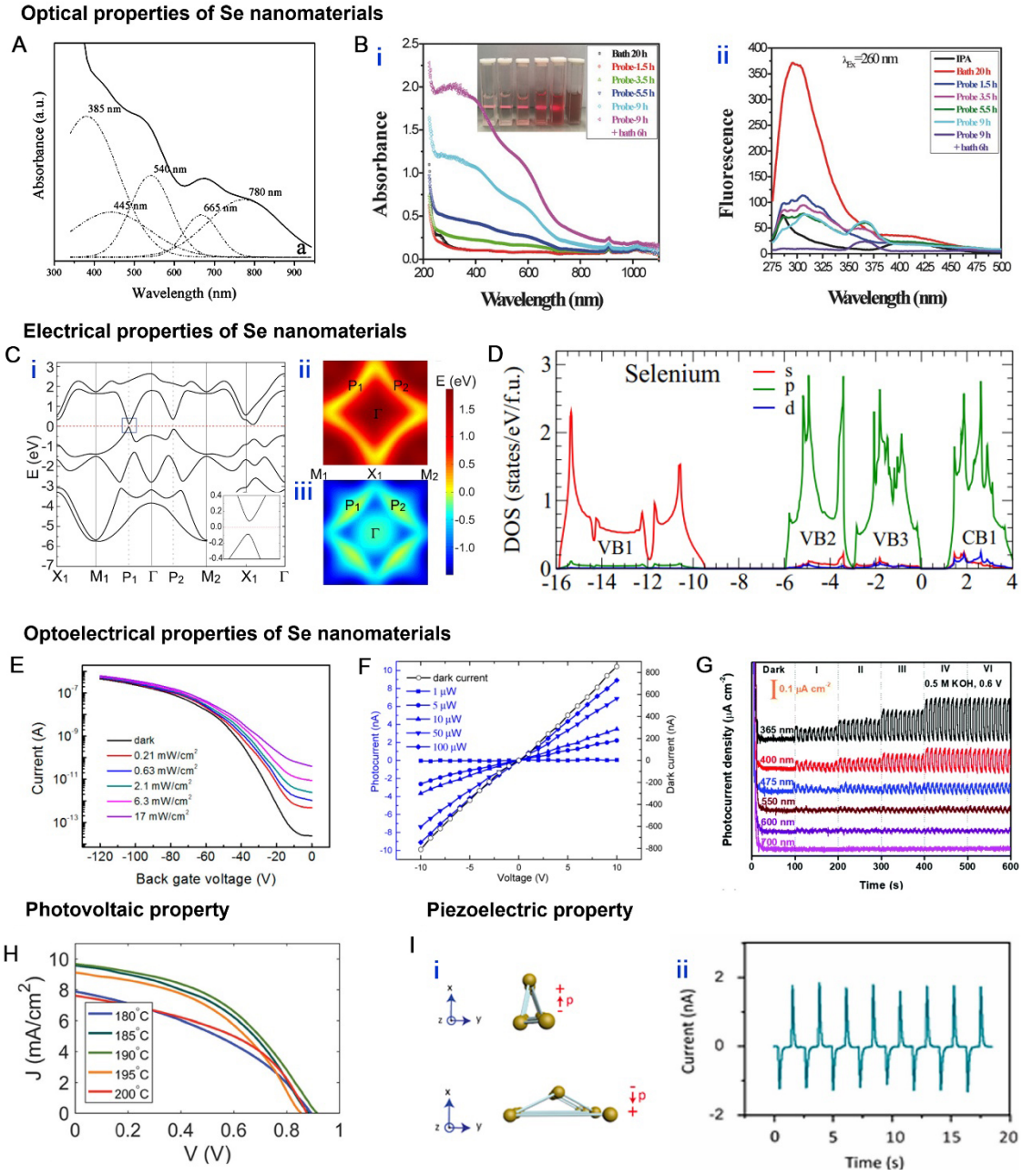

Figure 5. (A) Room temperature UV-vis absorption spectrum[72]; Copyright 2010, American Chemical Society. (B) (i) UV-vis absorption spectrum; (ii) Fluorescence spectra with an excitation wavelength of 260 nm[58]; Copyright 2017, Wiley-VCH. (C) (i) Band structure; (ii) and (iii) Band contour for the bottom conduction band (upper panel) and the top valence band (lower panel) in the first Brillouin zone[61]; Copyright 2019; IOP Publishing. (D) Total and orbital-projected density of states (DOS) for Se[73]; Copyright 2019, American Physical Society. (E) Transfer curves of a Se nanosheet phototransistor measured under various laser irradiation powers at V_{ds} = 3 V[57]; Copyright 2017, American Chemical Society. (F) Photocurrent as a function of laser illumination power measured from voltage of -10 V to 10 V[77]; Copyright 2017, Optical publishing group. (G) Photo response behaviors under lasers with various wavelengths and various laser power densities of dark and levels in 0.5 M KOH at a bias voltage of 0.6 V[78]; Copyright 2020, Royal society of chemistry. (H) *J-V* curves of Se-devices annealed at different specific temperatures[81]; Copyright 2019, Wiley-VCH. (I) (i) Schematic showing the deformed Se nanowire chain and the origin of the piezoelectric polarization; (ii) Short-circuit current (I_{sc}) of Se-PENGs[85]; Copyright 2015, Elsevier.

Moreover, Se nanoflakes presented a centrosymmetric structure possessing a spontaneous in-plane ferroelectric polarization of about 2.68 × 10^{-10} cm^{-1} per layer, which is favorable in nanoscale electronic devices. First-principles calculations revealed that two-dimensional layered Se structure exhibited two gapped semi-Dirac cones in the square Brillouin zone, indicating that they were topological insulators with nontrivial topological properties[61]. The Brillouin zone had Dirac-cone-like dispersion at P1. However, these band distributions showed significant anisotropy at the band contours around P1 [Figure 5C (i)-(iii)]. A density-functional-theory method was conducted to calculate the total and orbital projected densities of states of the trigonal Se[73]. As shown in Figure 5D, the lowest valence band ranging from -15.9 to -9.5 eV can be found in the VB1 region. VB2/VB3 and CB1 regions can also be observed in upper valence bands and lower conduction bands, respectively. A great deal of potential for the development and application of trigonal Se in linear electro-optic devices has thus been suggested.

Taking advantages of high photoconductivity, electrical anisotropy, and nonlinear optical properties, Se nanomaterials show great potential in optoelectrical applications[73-77]. Figure 5E shows the optoelectronic property of a phototransistor based on Se nanosheets[57]. The current-gate voltage curves show a gate tunability, where a photocurrent of up to 54 nA is generated even at a low illumination power of 0.21 mW cm^{-2}. This result indicates an excellent photoresponsivity of Se nanosheets. Control over the grain size of Se can further increase the optoelectronic performance. For example, a laser-based annealing approach enabled a polycrystalline domain where the grain size was a few micrometers in the direction perpendicular to the electric field while the grain size was much smaller in the direction of illumination, which led to a super-sensitive photodetector with performance on par with some planar nanoscale devices [Figure 5F][77]. Besides 2D and 3D Se nanomaterials, 0D Se nanomaterials, such as Se quantum dots, also show excellent optoelectronic properties. As shown by Figure 5G, the photocurrent is detected in Se quantum dots under an applied bias voltage of 0.6 V[78]. Notably, the potential gradient generated within Se quantum dots promoted the separation of electrons and holes, thus enabling a higher photocurrent density (1.80 μA cm^{-2}) than photodetectors based on Se nanosheets or Se nanowires.

Since its deployment in solar cells about 140 years ago, Se has been acting as a promising semiconducting material for the fabrication of photovoltaic devices[79,80]. Modulating crystalline structure can be an approach to improving solar cell efficiency. The relationship between solar cell performance and Se crystalline structure was investigated by Hadar *et al.*[81]. The presence of small crystal grains in Se's structure, as shown in Figure 5H, contributed to the low short-circuit current density (J_{sc}), which could be explained by the low orientation order of the crystals. In addition, another efficient strategy to improve high solar cell efficiency is incorporating Se with other metal elements, such as germanium (Ge), copper (Cu), and indium (In)[82-84].

Piezoelectric properties are also discovered in Se nanomaterials. Se nanowires exhibit strong piezoelectric properties due to the anisotropic crystal structure of the trigonal phase [Figure 5I][85]. When longitudinal stress is applied along the x-axis, the Se atoms undergo internal displacement and the electronic charge is displaced against the Se cores, resulting in piezoelectric polarization parallel to the x-axis. When Se nanowires are stretched (compressed) vertically, piezoelectric polarization pointing upward (downward) is generated [Figure 5I (i)]. As a result, short-circuit current (I_{sc}) is generated by compressing the Se nanowires along the alignment direction, showing a good perspective for piezoelectric nanogenerators [Figure 5I (ii)].

APPLICATIONS OF SELENIUM NANOMATERIALS IN FLEXIBLE AND WEARABLE ELECTRONICS

Several recent studies have demonstrated that Se nanomaterials represent an intriguing class of functional materials in flexible and wearable electronics because of their anisotropic structure, quantum confinement effects, large surface areas, and interesting optical, electrical, optoelectronic, electrochemical, photovoltaic,

and piezoelectric properties. This section summarizes and discusses the fabrication and application of Se nanomaterials-based flexible or wearable electronics, including flexible and wearable sensors for photedetection, mechanical deformation sensing and physiological sensing, and flexible batteries.

Flexible and wearable sensors for biomedicine and healthcare

Selenium is an intriguing optoelectronic material, and its bulk form has been used for a myriad of optoelectronic applications in xerography, ultrasensitive imaging, chemical detection and photodiodes[86-89]. Selenium nanowires with a trigonal phase offer more appealing optoelectronic properties over their bulky form[90,91]. The integration of trigonal selenium nanowires into flexible devices is bringing novel opportunities for smart sensing, surgical tools and optogenetics[92,93]. The iterative thermal drawing discussed in the previous section enabled ultralong Se nanowire array to align along the fiber length. Interfacing the nanowires at the two extremities of the fiber with external electrodes formed a fiber-based photodetector that was sensitive to visible light[70]. However, the in-fiber selenium exhibited either an amorphous or a polycrystalline structure. The disorganized atomic arrangement and crystal defects like grain boundaries act as recombination centers for charge carriers, hindering the charge collection and reducing the photosensitivity and photoresponsivity. Yan *et al.* have recently devised a novel method that combines thermal drawing and sonochemical synthesis to create flexible fiber-based optoelectronic devices made of single-crystal semiconducting nanowires [Figure 6A][39]. The bulk in-fiber Se underwent a transformation into a dense array of nanowires through the manipulation of the anisotropy in the surface energy of the crystal's crystal planes. The growth of single crystal nanowires from the amorphous bulk in 1-propanol resulted in the formation of in-fiber optoelectronic devices with built-in electrodes in intimate contact. These fiber devices showcased exceptional optical and optoelectronic performances, including high photoresponsivity and photosensitivity, low dark current, low noise-equivalent power, and ultrafast response speed, which rivaled many wafer-based devices. Notably, this innovative approach enabled high-throughput integration of nanowires into devices on an ultra-large scale, eliminating the need for intricate clean room contacting procedures. This was demonstrated through the growth of high-performance nanowire-based devices along the fiber length. The integration of multiple Se nanowire-based photodetectors and an optical fiber resulted in a hybrid fiber [Figure 6B][70]. The unique capability of this technology for fluorescent bioimaging based on the single multimodal fiber exhibiting simultaneous efficient optical guidance and excellent photodetection performance was demonstrated. The outstanding performance of the Se nanowires was analyzed to uncover the underlying mechanism. Ultrafast transient absorption spectroscopy, nanosecond flash photolysis, and time-resolved terahertz spectroscopy were used to study the charge carrier dynamics and mobility of Se nanowire meshes[11,31]. These noninvasive, contact-free methods uncovered a picosecond lifetime for free carriers and a microsecond lifetime for trapped carriers, both limited by trap-assisted recombination. Additionally, a high free carrier mobility of approximately 3.0 $cm^2 V^{-1} s^{-1}$ was discovered.

Due to their flexibility, small cross-section and high aspect ratio, fiber-shaped selenium nanowire optoelectronics are particularly useful for minimally invasive bioimaging, and remote and distributed photodetection. In addition to the fiber form factor, the selenium nanomaterials can also be integrated into large-area planar devices. Luo *et al.* reported fabrication of a thin film-based photodetector with full transparency and flexibility, in which the individual Se nanobelts were deposited on a flexible polyethylene terephthalate (PET) matrix [Figure 6C][94]. A number of characteristics were demonstrated to be impressive, including excellent transparency and flexibility, high light sensitivity, and stable response under various bending conditions.

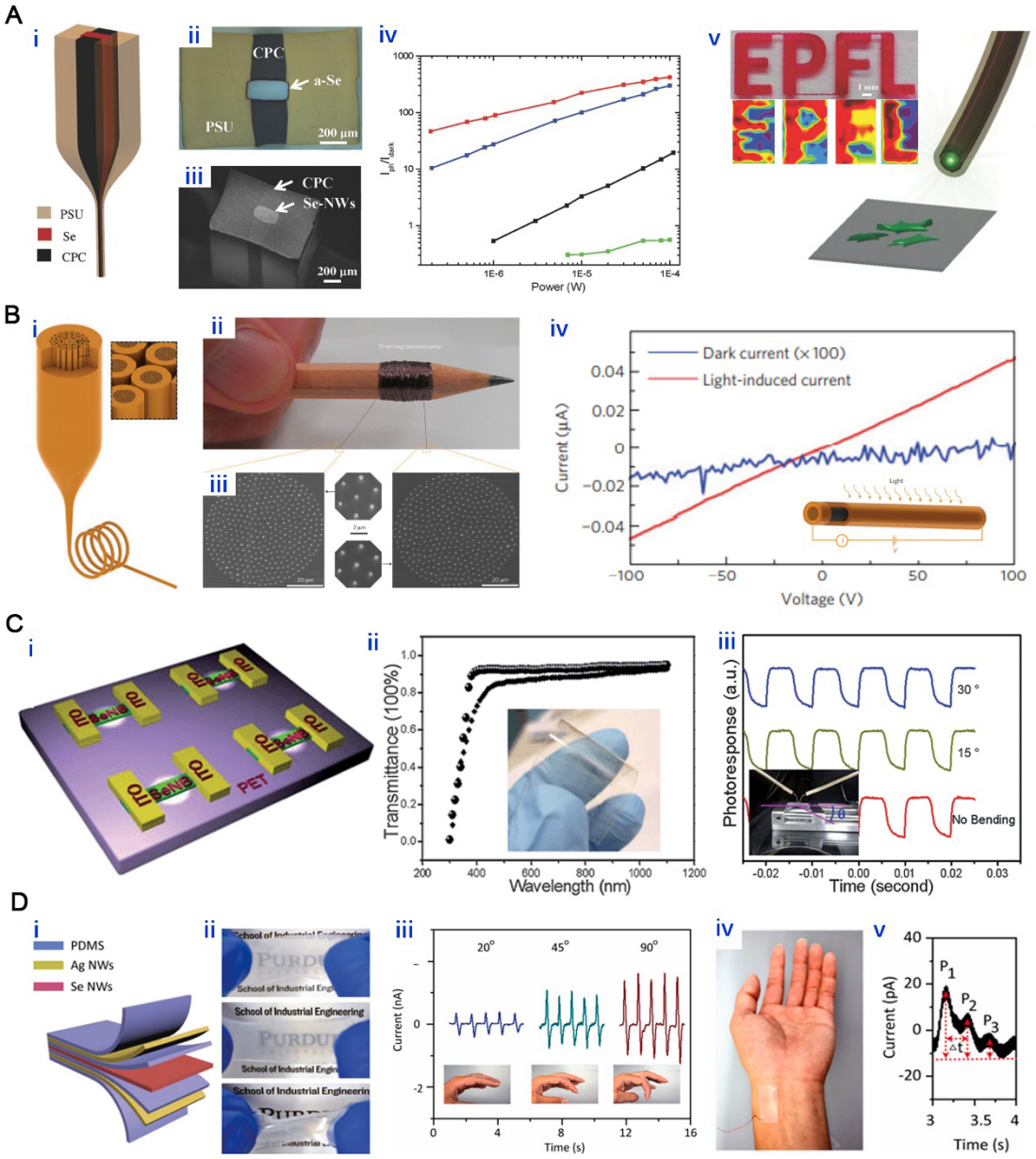

Figure 6. (A) (i) Schematic of multimaterials thermal drawing; (ii) Optical photograph of the cross section of the as-drawn fiber; (iii) SEM image of the fiber cross section after Se-nanowire formation;) Ratio I_{ph}/I_{dark} versus power for the same fibers;) Schematic of the fluorescence imaging system. Top: photograph of the "EPFL" logo filled with dye Rhodamine B dissolved in ethanol; bottom: fluorescent image obtained with the hybrid fiber device[39]; Copyright 2017, Wiley-VCH. (B) (i) Fabrication technique based on iterative size reduction to produce ordered, indefinitely long nanowire and nanotube arrays; (ii) A polymer-embedded nanowire array rolled around a pencil; (iii) Cross-sectional SEM micrographs from both sides of a 10-m-long polymer fibre that contains hundreds of nanowires; (iv) The photoconductance from a selenium nanowire in the dark and on white-light illumination[70]; Copyright 2011, Nature Publishing Group. (C) (i) Schematic illustration of the Se nanobelts photodetectors on transparent and flexible PET film; (ii) Optical transmittance spectra of Se nanobelts photodetector, the inset shows a picture of the photodetectors on PET film; (iii) Photoresponse of the photodetector a PET substrate with different bending angles, the inset shows a picture of the bending setup[94]; Copyright 2012, Royal society of chemistry. (D) (i) 3D illustration of the Se-PENG device; (ii) Optical images of the device in the original state, being stretched and twisted, respectively; (iii) The output current of the Se-PENG attached on the human fingers and bent with different angles; (iv) and (v) The real-time artery pulse signal monitored by the Se-PENG[85]; Copyright 2015, Elsevier.

By leveraging the piezoelectric property, selenium nanomaterials serve as excellent wearable sensors for mechanical deformation and physiological diagnosis. Wu *et al.* developed a Se nanowire-based piezoelectric nanogenerator (PENG) that consisted of PDMS layers, electrodes derived from Ag nanowires, and piezoelectric Se nanowires, as presented in Figure 6D[85]. Here, the PDMS layer serves two purposes: one is to act as the insulating layer between the Se and Ag nanowires, and the other is to encapsulate the Se and Ag nanowires to prevent oxidation and performance deterioration [Figure 6D (i)]. This device was flexible, stretchable, and robust enough to withstand mechanical deformation without breaking. Therefore, PENGs could be adhered to the skin of the human body to detect very faint deformations such as finger bending. The piezoelectric output voltage increases with the bending angle, allowing the finger movement to be recognized. Moreover, the nanogenerator could also be attached to a human wrist to detect the pulses of the radial artery in real time. Three distinct peaks are observed in the piezoelectric current output curve for the cardiac cycle. The P1, P2, and P3 represent the early systolic peak pressure, late systolic augmentation shoulder, and diastolic pulse waveform, respectively. These peaks can be valuable indicators to quantify the physiological information about the cardiovascular system of the wearer.

Flexible batteries

Recent studies have also demonstrated the huge potential of Se nanomaterials for high-performance electrodes in energy storage devices. Typical lithium-sulfur (Li-S) batteries show high theoretical specific capacities and energy densities. However, two major issues have hindered their practical application. First, sulfur is not a preferable electrode material because of its low electronic and ionic conductivity. Second, electrolyte-soluble polysulfide intermediate products are dissolvable in liquid electrolytes when a battery is working, leading to the significant shuttle effect and capacity loss[95-98].

Se is an alternative to sulfur and has been used as a potential electrode material for Li-Se batteries[99-101]. However, bulky Se cathodes exhibit poor cycle performance and low Coulombic efficiency in comparison with S cathodes[102]. One strategy to overcome this issue is to incorporate Se into a 3D interconnected mesoporous carbon nanofibers (CNFs)[103]. This nanostructured Se/CNF enabled high-performance electrodes [Figure 7A]. The resulting Li-Se batteries can deliver a reversible capacity of 516 mAh g^{-1} after 900 cycles without any capacity loss at 0.5 A g^{-1}.

Moreover, self-standing nanostructured graphene-Se@CNT film electrodes for Li-Se batteries have been synthesized[104]. The electrode displays high flexibility and bendability, as shown in Figure 7B. The flexible film cathode delivers a high reversible discharge capacity of 400 mAh g^{-1} that is slightly reduced to 315 mAh g^{-1}, as well as a stable Coulombic efficiency above 96% even after 100 charging-discharging cycles. Nanostructured Se has also been integrated into Na-Se batteries for improved performance. For example, impregnating Se into microporous multichannel carbon nanofibers (MCNF) forms a self-standing cathode film in a Na-Se battery [Figure 7C] that exhibits an extraordinary discharge capacity (596 mA h g^{-1} at the 100th cycle at 0.1 A g^{-1}), excellent rate capability (379 mA h g^{-1} at 2 A g^{-1}), and long-time capacity durability over 300 charging-discharging cycles[105]. With more advances in performance, flexible batteries based on nanostructured Se might constitute a powerful platform for powering flexible and electronic devices and systems instead of using conventional heavy and rigid counterparts.

CONCLUSION AND OUTLOOK

Se nanomaterials are experiencing a flourishing research momentum. Advances in materials synthesis and fabrication, control over morphologies and structure, fundamental understanding of structure-properties relationship, and methodologies of devices integration offer a new class of Se nanomaterial-based flexible and wearable electronics, with wide-ranging applications in smart sensing, health care and energy. While the translation of nanoscale materials into macroscopic real devices is truly exciting, some challenges relevant to fundamental and applied science still exist.

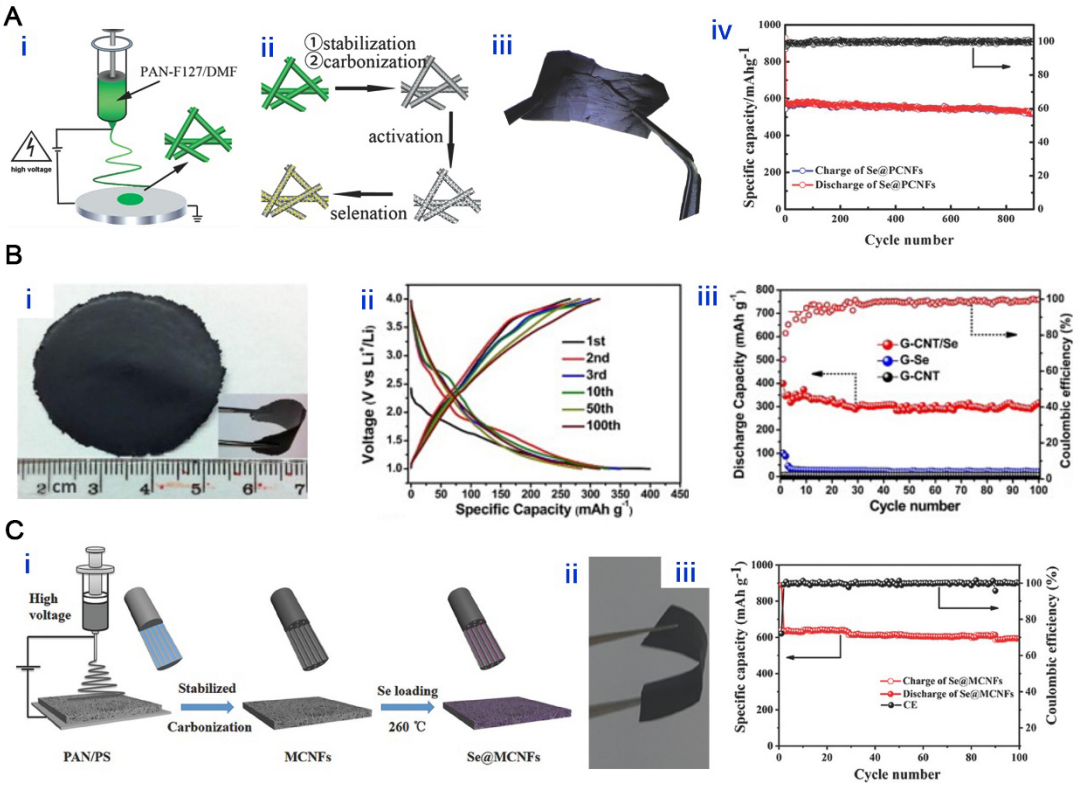

Figure 7. (A) (i) and (ii) Schematic illustration of the synthesis process of the Se@PCNFs electrode; (iii) Photograph of free-standing and flexible Se@PCNFs electrode; (iv) Long-term cycling performance of Se@PCNFs electrode in Li-ion batteries at 0.5 A g^{-1} for 900 cycles[103]; Copyright 2015, Wiley-VCH. (B) (i) Digital photo of the flexible self-standing graphene-Se@CNT composite film; (ii) Charge/discharge profiles of the graphene-Se@CNT composite film with cycles at 0.1 C current rate; (iii) Cycling performance of the self-standing graphene-Se@CNT at 0.1 C[104]; Copyright 2014, Elsevier. (C) (i) Schematic illustration of the synthesis process for Se@MCNF electrode; (ii) photograph of flexible and freestanding Se@MCNF electrode; (iii) Cyclic performances of the Se@MCNF electrode at a current density of 0.1 A g^{-1} and coulombic efficiency during cycling[105]; Copyright 2017, Wiley-VCH.

Synthesis and fabrication: The fabrication of high-performance Se nanomaterial-based flexible and wearable electronic devices relies on the precise positioning and alignment of Se nanomaterials. Most existing approaches to Se nanomaterials synthesis are built upon solution-based processes that involve complex chemical reactions, producing Se nanomaterials with irregular positioning and agglomeration or entanglement. The fabrication of well-ordered, highly uniform Se nanomaterials remains a significant challenge. Moreover, the solution-based approaches, for the most part, exploit noxious raw materials such as Na_2SeO_3 and H_2SeO_3. Their inappropriate handling poses a significant threat to the environment. While solution-free methods such as PVD and CVT only process bulky Se, fulfilling the requirements of high temperature, high-vacuum environment, and highly purified gases demands high operation costs, which undermines the possibility of large-scale production. More controllable, effective, and eco-friendly synthesis and fabrication methods are heavily needed. The recent innovation in harnessing the multimaterial thermal drawing platform has demonstrated a unique and powerful platform for manufacturing periodic arrays of Se nanomaterials in an unprecedentedly green, sustainable and scalable manner[70,76,106-108]. The research along this direction has just begun and is expected to be an exciting paradigm for next-generation Se nanomaterial-based flexible and wearable electronics.

Structure-properties correlation: Se nanomaterials exhibit many intriguing optical, electrical, optoelectronic, photovoltaic, and piezoelectric properties. However, a deep understanding of the structure-properties correlation is still very limited. Harnessing sophisticated characterization techniques such as ultrafast transient absorption spectroscopy, nanosecond flash photolysis and time-resolved terahertz spectroscopy has paved a novel way toward this research direction[31]. This would allow us, on the one hand, to unravel the working principles of Se nanomaterial-based devices and, on the other hand, conversely tune the material structure to further improve performance.

Materials assembly and device integration: Most existing Se nanomaterials suffer from agglomeration or entanglement. Therefore, it requires a stringent post-synthesis process for materials alignment, assembly and device integration. Even though thermal drawing produces well-aligned and exquisitely controllable in-fiber nanomaterials, their monolithic integration with other functional materials such as electrodes for the fabrication of flexible and wearable electronic devices remains challenging. The difficulty is twofold: the co-drawing of Se with other functional materials is challenging because of their incompatible rheological properties; handling materials at the nanoscale is complicated. Nevertheless, an initial step with innovative advances in in-fiber nanowire self-assembly and simultaneous integration with built-in electrodes offers an appealing inspiration for us to further break through the roadblock[39]. More simpler and robust strategies for Se nanomaterials assembly and device integration are desirable for future real-world applications.

Se nanomaterial-based flexible and wearable electronics represent a class of technology with innovative potentials in smart sensing, health care and energy. With continued and concerted efforts in synthesis and fabrication, control over morphologies and structure, device assembly and integration, more advanced flexible and wearable electronics with more sophisticated functionalities and practical applications will emerge.

DECLARATIONS

Authors' contributions

Made substantial contributions to the conception and design of the study: Dang C, Yan W
Writing-original draft preparation and review editing: Dang C, Liu M, Lin Z, Yan W

Availability of data and materials

Not applicable.

Financial support and sponsorship

Yan W acknowledges the Nanyang Technological University (Start-up Grant 021850-00001: Yan W) and the National Natural Science Foundation of China (Grant No. 52202167).

Conflicts of interest

All authors declared that there are no conflicts of interest.

Ethical approval and consent to participate

Not applicable.

Consent for publication

Not applicable.

REFERENCES

1. Yan W, Noel G, Loke G, et al. Single fibre enables acoustic fabrics via nanometre-scale vibrations. *Nature* 2022;603:616-23. DOI PubMed
2. Yan W, Dong C, Xiang Y, et al. Thermally drawn advanced functional fibers: new frontier of flexible electronics. *Mater Today* 2020;35:168-94. DOI
3. Zeng W, Shu L, Li Q, Chen S, Wang F, Tao XM. Fiber-based wearable electronics: a review of materials, fabrication, devices, and applications. *Adv Mater* 2014;26:5310-36. DOI PubMed
4. Leber A, Dong C, Chandran R, Das Gupta T, Bartolomei N, Sorin F. Soft and stretchable liquid metal transmission lines as distributed probes of multimodal deformations. *Nat Electron* 2020;3:316-26. DOI
5. Song W. A smart sensor that can be woven into everyday life. *Nature* 2022;603:585-6. DOI PubMed
6. Du M, Huang L, Zheng J, et al. Flexible fiber probe for efficient neural stimulation and detection. *Adv Sci (Weinh)* 2020;7:2001410. DOI PubMed PMC
7. Weng W, Yang J, Zhang Y, et al. A route toward smart system integration: from fiber design to device construction. *Adv Mater* 2020;32:e1902301. DOI PubMed
8. Loke G, Alain J, Yan W, et al. Computing fabrics. *Matter* 2020;2:786-8. DOI
9. Liu M, Lin Z, Wang X, et al. Focused rotary jet spinning: a novel fiber technology for heart biofabrication. *Matter* 2022;5:3576-9. DOI
10. Jiang S, Patel DC, Kim J, et al. Spatially expandable fiber-based probes as a multifunctional deep brain interface. *Nat Commun* 2020;11:6115. DOI PubMed PMC
11. Xu B, Ma S, Xiang Y, et al. In-fiber structured particles and filament arrays from the perspective of fluid instabilities. *Adv Fiber Mater* 2020;2:1-12. DOI
12. Pan S, Zhu M. Nanoprocessed silk makes skin feel cool. *Adv Fiber Mater* 2022;4:319-20. DOI
13. Wang H, Zhang Y, Liang X, Zhang Y. Smart fibers and textiles for personal health management. *ACS Nano* 2021;15:12497-508. DOI PubMed
14. Zhang T, Li K, Zhang J, et al. High-performance, flexible, and ultralong crystalline thermoelectric fibers. *Nano Energy* 2017;41:35-42. DOI
15. Martin-monier L, Gupta TD, Yan W, Lacour S, Sorin F. Nanoscale controlled oxidation of liquid metals for stretchable electronics and photonics. *Adv Funct Mater* 2021;31:2006711. DOI
16. Pan S, Zhu M. Fiber electronics bring a new generation of acoustic fabrics. *Adv Fiber Mater* 2022;4:321-3. DOI
17. Qian S, Liu M, Dou Y, Fink Y, Yan W. A 'Moore's law' for fibers enables intelligent fabrics. *Natl Sci Rev* 2023;10:nwac202. DOI PubMed PMC
18. Loke G, Khudiyev T, Wang B, et al. Digital electronics in fibres enable fabric-based machine-learning inference. *Nat Commun* 2021;12:3317. DOI PubMed PMC
19. Kim J, Jia X. From space to battlefield: a new breed of multifunctional fiber sheets for extreme environments. *Matter* 2020;3:602-4. DOI
20. Cao Y, Wu H, Allec SI, Wong BM, Nguyen DS, Wang C. A highly stretchy, transparent elastomer with the capability to automatically self-heal underwater. *Adv Mater* 2018;30:e1804602. DOI PubMed
21. Hou C, Jia X, Wei L, et al. Crystalline silicon core fibres from aluminium core preforms. *Nat Commun* 2015;6:6248. DOI PubMed
22. Wei L, Hou C, Levy E, et al. Optoelectronic fibers via selective amplification of in-fiber capillary instabilities. *Adv Mater* 2017;29:1603033. DOI PubMed
23. Qu Y, Nguyen-Dang T, Page AG, et al. Superelastic multimaterial electronic and photonic fibers and devices via thermal drawing. *Adv Mater* 2018;30:e1707251. DOI PubMed
24. Yan W, Burgos-caminal A, Das Gupta T, Moser J, Sorin F. Direct synthesis of selenium nanowire mesh on a solid substrate and insights into ultrafast photocarrier dynamics. *J Phys Chem C* 2018;122:25134-41. DOI
25. Chin AL, Jiang S, Jang E, et al. Implantable optical fibers for immunotherapeutics delivery and tumor impedance measurement. *Nat Commun* 2021;12:5138. DOI PubMed PMC
26. Dong C, Leber A, Das Gupta T, et al. High-efficiency super-elastic liquid metal based triboelectric fibers and textiles. *Nat Commun* 2020;11:3537. DOI PubMed PMC
27. Cao Y, Morrissey TG, Acome E, et al. A Transparent, self-healing, highly stretchable ionic conductor. *Adv Mater* 2017;29:1605099. DOI PubMed
28. Yan W, Richard I, Kurtuldu G, et al. Structured nanoscale metallic glass fibres with extreme aspect ratios. *Nat Nanotechnol* 2020;15:875-82. DOI PubMed
29. Nguyen-dang T, de Luca AC, Yan W, et al. Controlled sub-micrometer hierarchical textures engineered in polymeric fibers and microchannels via thermal drawing. *Adv Funct Mater* 2017;27:1605935. DOI
30. Zhang Y, Li X, Kim J, et al. Thermally drawn stretchable electrical and optical fiber sensors for multimodal extreme deformation

sensing. *Adv Optical Mater* 2021;9:2001815. DOI

31. Jiang S, Song J, Zhang Y, et al. Nano-optoelectrodes integrated with flexible multifunctional fiber probes by high-throughput scalable fabrication. *ACS Appl Mater Interfaces* 2021;13:9156-65. DOI PubMed
32. Das Gupta T, Martin-Monier L, Yan W, et al. Self-assembly of nanostructured glass metasurfaces via templated fluid instabilities. *Nat Nanotechnol* 2019;14:320-7. DOI PubMed
33. Kim J, Zhao Y, Yang S, et al. Laser machined fiber-based microprobe: application in microscale electroporation. *Adv Fiber Mater* 2022;4:859-72. DOI
34. Dong C, Page AG, Yan W, Nguyen-dang T, Sorin F. Microstructured multimaterial fibers for microfluidic sensing. *Adv Mater Technol* 2019;4:1900417. DOI
35. Grena B, Alayrac JB, Levy E, Stolyarov AM, Joannopoulos JD, Fink Y. Thermally-drawn fibers with spatially-selective porous domains. *Nat Commun* 2017;8:364. DOI PubMed PMC
36. Sun H, Xie S, Li Y, et al. Large-area supercapacitor textiles with novel hierarchical conducting structures. *Adv Mater* 2016;28:8431-8. DOI PubMed
37. Khudiyev T, Lee JT, Cox JR, et al. 100 m long thermally drawn supercapacitor fibers with applications to 3D printing and textiles. *Adv Mater* 2020;32:e2004971. DOI PubMed
38. Zhang J, Zhang T, Zhang H, et al. Single-crystal snse thermoelectric fibers via laser-induced directional crystallization: from 1d fibers to multidimensional fabrics. *Adv Mater* 2020;32:e2002702. DOI PubMed
39. Yan W, Qu Y, Gupta TD, et al. Semiconducting nanowire-based optoelectronic fibers. *Adv Mater* 2017;29:1700681. DOI PubMed
40. Hou C, Jia X, Wei L, et al. Direct atomic-level observation and chemical analysis of ZnSe synthesized by in situ high-throughput reactive fiber drawing. *Nano Lett* 2013;13:975-9. DOI PubMed
41. Zhang H, li L, Zheng D, et al. Broadband photodetector based on vapor-deposited selenium self-supporting films. *Ceramics International* 2022;48:27750-7. DOI
42. Shalaev VM. Physics Transforming light. *Science* 2008;322:384-6. DOI PubMed
43. Hu K, Chen H, Jiang M, Teng F, Zheng L, Fang X. Broadband photoresponse enhancement of a high-performance *t* -Se microtube photodetector by plasmonic metallic nanoparticles. *Adv Funct Mater* 2016;26:6641-8. DOI
44. Kumar M, Dubey A, Adhikari N, Venkatesan S, Qiao Q. Strategic review of secondary phases, defects and defect-complexes in kesterite CZTS-Se solar cells. *Energy Environ Sci* 2015;8:3134-59. DOI
45. Wang S, Liu X, Zhou P. The road for 2D semiconductors in the silicon age. *Adv Mater* 2022;34:e2106886. DOI PubMed
46. Kang SK, Park G, Kim K, et al. Dissolution chemistry and biocompatibility of silicon- and germanium-based semiconductors for transient electronics. *ACS Appl Mater Interfaces* 2015;7:9297-305. DOI PubMed
47. Khalid A, Tran PA, Norello R, Simpson DA, O'Connor AJ, Tomljenovic-Hanic S. Intrinsic fluorescence of selenium nanoparticles for cellular imaging applications. *Nanoscale* 2016;8:3376. DOI PubMed
48. Ramírez-montes L, López-pérez W, González-hernández R, Pinilla C. Large thermoelectric figure of merit in hexagonal phase of 2D selenium and tellurium. *Int J Quantum Chem* 2020:120. DOI
49. Qin JK, Zhou F, Wang J, Chen J, et al. Anisotropic signal processing with trigonal selenium nanosheet synaptic transistors. *ACS Nano* 2020;14:10018-26. DOI PubMed
50. Huang W, Wang M, Hu L, Wang C, Xie Z, Zhang H. Recent advances in semiconducting monoelemental selenium nanostructures for device applications. *Adv Funct Mater* 2020;30:2003301. DOI
51. Kumar A, Sevonkaev I, Goia DV. Synthesis of selenium particles with various morphologies. *J Colloid Interf Sci* 2014;416:119-123. DOI PubMed
52. Gao X, Zhang J, Zhang L. Hollow sphere selenium nanoparticles: their *in-vitro* anti hydroxyl radical effect. *Adv Mater* 2002;14:290-3. DOI
53. Zhang J, Xu Y, Fan L, Zhu Y, Liang J, Qian Y. Graphene-encapsulated selenium/polyaniline core-shell nanowires with enhanced electrochemical performance for Li-Se batteries. *Nano Energy* 2015;13:592-600. DOI
54. Zhu Y, Hu X. Preparation of powders of selenium nanorods and nanowires by microwave-polyol method. *Mater Lett* 2004;58:1234-6. DOI
55. Xi G, Xiong K, Zhao Q, Zhang R, Zhang H, Qian Y. Nucleation-dissolution-recrystallization: a new growth mechanism for *t* -selenium nanotubes. *Crystal Growth & Design* 2006;6:577-82. DOI
56. Ma Y, Qi L, Shen W, Ma J. Selective synthesis of single-crystalline selenium nanobelts and nanowires in micellar solutions of nonionic surfactants. *Langmuir* 2005;21:6161-4. DOI PubMed
57. Qin J, Qiu G, Jian J, et al. Controlled growth of a large-size 2D selenium nanosheet and its electronic and optoelectronic applications. *ACS Nano* 2017;11:10222-9. DOI PubMed
58. Xing C, Xie Z, Liang Z, et al. 2D Nonlayered selenium nanosheets: facile synthesis, photoluminescence, and ultrafast photonics. *Adv Optical Mater* 2017;5:1700884. DOI
59. Shi Z, Zhang H, Khan K, Cao R, Xu K, Zhang H. Two-dimensional selenium and its composites for device applications. *Nano Res* 2022;15:104-22. DOI
60. Liu C, Hu T, Wu Y B, et al. 2D selenium allotropes from first principles and swarm intelligence. *J Phys Condens Matter* 2019;31:235702. DOI PubMed
61. Xian L, Pérez Paz A, Bianco E, Ajayan PM, Rubio A. Square selenene and tellurene: novel group VI elemental 2D materials with

nontrivial topological properties. *2D Mater* 2017;4:041003. DOI

62. Degtyareva O, Gregoryanz E, Somayazulu M, Mao H, Hemley RJ. Crystal structure of the superconducting phases of S and Se. *Phys Rev B* 2005;71:214104. DOI
63. Cherin P, Unger P. The crystal structure of trigonal selenium. *Inorg Chem* 1967;6:1589-91. DOI
64. Anupama K, Paul T, Mary KAA. Solid-state fluorescent selenium quantum dots by a solvothermal assisted sol-gel route for curcumin sensing. *ACS Omega* 2021;6:21525-33. DOI PubMed PMC
65. Ayyyzhy KO, Voronov VV, Gudkov SV, Rakov II, Simakin AV, Shafeev GA. Laser fabrication and fragmentation of selenium nanoparticles in aqueous media. *Phys Wave Phen* 2019;27:113-8. DOI
66. Salazar-alvarez G, Muhammed M, Zagorodni AA. Novel flow injection synthesis of iron oxide nanoparticles with narrow size distribution. *Chem Eng Sci* 2006;61:4625-33. DOI
67. Basak S, Chen D, Biswas P. Electrospray of ionic precursor solutions to synthesize iron oxide nanoparticles: modified scaling law. *Chem Eng Sci* 2007;62:1263-8. DOI
68. Gates B, Mayers B, Cattle B, Xia Y. Synthesis and characterization of uniform nanowires of trigonal selenium. *Adv Funct Mater* 2002;12:219. DOI
69. Chen YZ, You YT, Chen PJ, et al. Environmentally and mechanically stable selenium 1D/2D hybrid structures for broad-range photoresponse from ultraviolet to infrared wavelengths. *ACS Appl Mater Interfaces* 2018;10:35477-86. DOI PubMed
70. Yaman M, Khudiyev T, Ozgur E, et al. Arrays of indefinitely long uniform nanowires and nanotubes. *Nat Mater* 2011;10:494-501. DOI PubMed
71. Kasirga TS. Chemical vapor transport synthesis of a selenium-based two-dimensional material. *Turk J Phys* 2018:42. DOI
72. Filippo E, Manno D, Serra A. Characterization and growth mechanism of selenium microtubes synthesized by a vapor phase deposition route. *Crystal Growth & Design* 2010;10:4890-7. DOI
73. Cheng M, Wu S, Zhu Z, Guo G. Large second-harmonic generation and linear electro-optic effect in trigonal selenium and tellurium. *Phys Rev B* 2019:100. DOI
74. Jun SW, Jeon S, Kwon J, Lee J, Kim C, Hong SW. Full-color laser displays based on optical second-harmonic generation from the thin film arrays of selenium nanowires. *ACS Photonics* 2022;9:368-77. DOI
75. Gumennik A, Stolyarov AM, Schell BR, et al. All-in-fiber chemical sensing. *Adv Mater* 2012;24:6005-9. DOI PubMed
76. Deng DS, Orf ND, Abouraddy AF, et al. In-fiber semiconductor filament arrays. *Nano Lett* 2008;8:4265-9. DOI PubMed
77. Yan W, Nguyen-dang T, Cayron C, et al. Microstructure tailoring of selenium-core multimaterial optoelectronic fibers. *Opt Mater Express* 2017;7:1388. DOI
78. Jiang X, Huang W, Wang R, et al. Photocarrier relaxation pathways in selenium quantum dots and their application in UV-Vis photodetection. *Nanoscale* 2020;12:11232-41. DOI PubMed
79. Shin D, Zhu T, Huang X, Gunawan O, Blum V, Mitzi DB. Earth-abundant chalcogenide photovoltaic devices with over 5% efficiency based on a Cu_2 $BaSn(S,Se)_4$ absorber. *Adv Mater* 2017;29:1606945. DOI PubMed
80. Jayswal NK, Rijal S, Subedi B, et al. Optical properties of thin film Sb_2Se_3 and identification of its electronic losses in photovoltaic devices. *Solar Energy* 2021;228:38-44. DOI
81. Hadar I, Song T, Ke W, Kanatzidis MG. Modern processing and insights on selenium solar cells: the world's first photovoltaic device. *Adv Energy Mater* 2019;9:1802766. DOI
82. Liu SC, Dai CM, Min Y, et al. An antibonding valence band maximum enables defect-tolerant and stable GeSe photovoltaics. *Nat Commun* 2021;12:670. DOI PubMed PMC
83. Seo Y, Lee B, Jo Y, et al. Facile microwave-assisted synthesis of multiphase $CuInSe_2$ nanoparticles and role of secondary cuse phase on photovoltaic device performance. *J Phys Chem C* 2013;117:9529-36. DOI
84. Ulaganathan RK, Yadav K, Sankar R, Chou FC, Chen Y. Hybrid InSe nanosheets and MoS_2 quantum dots for high-performance broadband photodetectors and photovoltaic cells. *Adv Mater Interfaces* 2019;6:1801336. DOI
85. Wu M, Wang Y, Gao S, et al. Solution-synthesized chiral piezoelectric selenium nanowires for wearable self-powered human-integrated monitoring. *Nano Energy* 2019;56:693-9. DOI
86. Harkin JM, Dong A, Chesters G. Elevation of selenium levels in air by xerography. *Nature* 1976;259:204-5. DOI PubMed
87. Zhu B, Wu L, Wang Y, et al. A highly selective and ultrasensitive ratiometric far-red fluorescent probe for imaging endogenous peroxynitrite in living cells. *Sensor Actuat B-Chem* 2018;259:797-802. DOI
88. Manjare ST, Kim Y, Churchill DG. Selenium- and tellurium-containing fluorescent molecular probes for the detection of biologically important analytes. *Acc Chem Res* 2014;47:2985-98. DOI PubMed
89. Triet Ho LT, Mukherjee A, Vasileska D, et al. Modeling dark current conduction mechanisms and mitigation techniques in vertically stacked amorphous selenium-based photodetectors. *ACS Appl Electron Mater* 2021;3:3538-46. DOI PubMed PMC
90. Liao ZM, Hou C, Liu LP, Yu DP. Temperature dependence of photoelectrical properties of single selenium nanowires. *Nanoscale Res Lett* 2010;5:926-9. DOI PubMed PMC
91. Luo LB, Jie JS, Chen ZH, et al. Photoconductive properties of selenium nanowire photodetectors. *J Nanosci Nanotechnol* 2009;9:6292-8. DOI PubMed
92. Akiyama N. A sensor array based on trigonal-selenium nanowires for the detection of gas mixtures. *Sensor Actuat B-Chem* 2016;223:131-7. DOI
93. Yan W, Page A, Nguyen-Dang T, et al. Advanced multimaterial electronic and optoelectronic fibers and textiles. *Adv Mater*

2019;31:e1802348. DOI PubMed

94. Luo L, Yang X, Liang F, et al. Transparent and flexible selenium nanobelt-based visible light photodetector. *CrystEngComm* 2012;14:1942. DOI
95. Ji L, Rao M, Zheng H, et al. Graphene oxide as a sulfur immobilizer in high performance lithium/sulfur cells. *J Am Chem Soc* 2011;133:18522-5. DOI PubMed
96. Bruce PG, Freunberger SA, Hardwick LJ, Tarascon JM. Li-O_2 and Li-S batteries with high energy storage. *Nat Mater* 2011;11:19-29. DOI PubMed
97. Luo C, Xu Y, Zhu Y, et al. Selenium@mesoporous carbon composite with superior lithium and sodium storage capacity. *ACS Nano* 2013;7:8003-10. DOI
98. Guo J, Xu Y, Wang C. Sulfur-impregnated disordered carbon nanotubes cathode for lithium-sulfur batteries. *Nano Lett* 2011;11:4288-94. DOI PubMed
99. Abouimrane A, Dambournet D, Chapman KW, Chupas PJ, Weng W, Amine K. A new class of lithium and sodium rechargeable batteries based on selenium and selenium-sulfur as a positive electrode. *J Am Chem Soc* 2012;134:4505-8. DOI PubMed
100. Liu L, Hou Y, Wu X, et al. Nanoporous selenium as a cathode material for rechargeable lithium-selenium batteries. *Chem Commun (Camb)* 2013;49:11515-7. DOI PubMed
101. Yang CP, Xin S, Yin YX, Ye H, Zhang J, Guo YG. An advanced selenium-carbon cathode for rechargeable lithium-selenium batteries. *Angew Chem Int Ed Engl* 2013;52:8363-7. DOI PubMed
102. Zhang Z, Zhang Z, Zhang K, Yang X, Li Q. Improvement of electrochemical performance of rechargeable lithium-selenium batteries by inserting a free-standing carbon interlayer. *RSC Adv* 2014;4:15489-92. DOI
103. Zeng L, Zeng W, Jiang Y, et al. A flexible porous carbon nanofibers-selenium cathode with superior electrochemical performance for both Li-Se and Na-Se batteries. *Adv Energy Mater* 2015;5:1401377. DOI
104. Han K, Liu Z, Ye H, Dai F. Flexible self-standing graphene-Se@CNT composite film as a binder-free cathode for rechargeable Li-Se batteries. *J Power Sources* 2014;263:85-9. DOI
105. Yuan B, Sun X, Zeng L, Yu Y, Wang Q. A Freestanding and long-life sodium-selenium cathode by encapsulation of selenium into microporous multichannel carbon nanofibers. *Small* 2018;14:1703252. DOI PubMed
106. Marion JS, Gupta N, Cheung H, Monir K, Anikeeva P, Fink Y. Thermally drawn highly conductive fibers with controlled elasticity. *Adv Mater* 2022;34:e2201081. DOI PubMed
107. Deng DS, Nave JC, Liang X, Johnson SG, Fink Y. Exploration of in-fiber nanostructures from capillary instability. *Opt Express* 2011;19:16273-90. DOI PubMed
108. Esposito W, Martin-Monier L, Piveteau PL, Xu B, Deng D, Sorin F. Controlled filamentation instability as a scalable fabrication approach to flexible metamaterials. *Nat Commun* 2022;13:6154. DOI PubMed PMC